High-Precision Relocation and Event Discrimination for the 3 September 2017 Underground Nuclear Explosion and Subsequent Seismic Events at the North Korean Test Site

by Xi He, Lian-Feng Zhao, Xiao-Bi Xie, and Zhen-Xing Yao

ABSTRACT

On 3 September 2017, a strong seismic event occurred at the North Korean nuclear test site near the border between China and North Korea. Using *P*/*S*-type spectral ratios calculated from regional seismic data, we identified this event as an explosion. Using a high-precision relative location method, with the first North Korean nuclear test as the master event, we obtained that the epicenter of this explosion was at 41.3018° N and 129.0696° E with a relative location precision of ~87 m based on the error ellipse. This explosion was followed by three moderate seismic events, which occurred 8 min after the explosion, on 23 September and 12 October 2017, respectively. The relocation suggests that the first postexplosion event occurred under the same mountain as the nuclear tests, but the other two events were located about 8 km to the northeast of the explosion. Based on their spectral ratios, these postexplosion events are clearly distinguished from the explosions.

Electronic Supplement: Table of *Pn* differential travel times at individual stations and figures of *Pn* waveforms recorded at YNB station and compared among North Korean test site (NKTS) events and spectral ratios from individual stations and events.

INTRODUCTION

According to the China Earthquake Network Center (CENC) and many other agencies, a possible explosion with magnitude m_b 6.3 (CENC) occurred in North Korea at 03:30 (UTC) on 3 September 2017 (Fig. 1). The strong shock from this event could be felt in China–North Korea border areas. The Democratic People's Republic of Korea claimed that it successfully detonated a fusion device, which was the sixth and the largest underground nuclear test, following previous tests in 2006, 2009, 2013, and January and September 2016. As illustrated in Figure 2, the waveforms from all six explosions were very similar and characterized by abrupt primary *P* waves, weak *Lg* phases, deficient *Sn* phases, and well-developed short-period Rayleigh waves, which are typical features of shallow explosions. After the explosion, three aftershocks occurred in the vicinity of the North Korean test site (NKTS) on 3 and 23 September and 12 October 2017, with magnitudes of $M_L = 4.1$, 3.5, and 2.9, respectively (U.S. Geological Survey [USGS]). These events were immediately suspected to be additional nuclear tests. Seismograms for these postexplosion events are illustrated at the bottom of Figure 2. The dominant frequencies and relative amplitudes of various phases generated by postexplosion events are different from those from explosions, suggesting different source time functions and focal mechanisms (Liu *et al.*, 2018; Tian *et al.*, 2018). Because of the large magnitude of the 3 September explosion, the aftershocks were speculated to be collapses of explosion cavities or induced tectonic earthquakes.

An abundance of broadband digital seismograms was generated by these events within regional distances. We collected seismic data from the China National Digital Seismic Network (CNDSN), Global Seismic Network (GSN), International Federation of Digital Seismograph Networks (FDSN), and Full Range Seismograph Network (F-net) in Japan to investigate characteristics of the 3 September 2017 explosion and three subsequent aftershocks (Fig. 1). Based on a relative location method (Schaff and Richards, 2004; Schlittenhardt *et al.*, 2010; Selby, 2010; Wen and Long, 2010; Murphy *et al.*, 2013; Zhang and Wen, 2013; Zhao, Xie, He, *et al.*, 2017; Zhao, Xie, Wang, *et al.*, 2017; Pasyanos and Myers, 2018; Xie and Zhao, 2018), we relocated the North Korean underground nuclear

 doi: 10.1785/0220180164

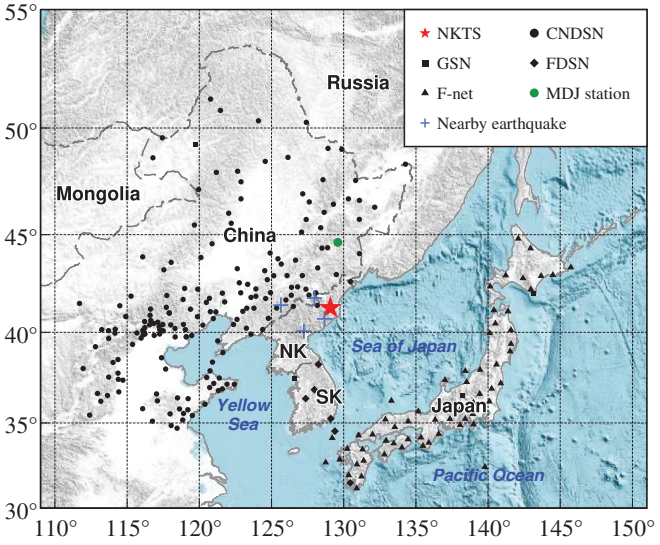

▲ **Figure 1.** Map showing the locations of the North Korean test site (NKTS) (solid red star), China National Digital Seismic Network (CNDSN), Global Seismic Network (GSN), International Federation of Digital Seismograph Networks (FDSN), and Full Range Seismograph Network (F-net) stations used for relocation in this study. Additionally, the MDJ station and four nearby natural earthquakes are also denoted. NK, North Korea; SK, South Korea.

tests and three postexplosion events. The epicenter of the 3 September 2017 explosion was ~3.6 km northwest of the master event, that is, the first nuclear test on 9 October 2006. Using the *P*/*S* spectral ratio method (e.g., Richards and Kim, 2007; Zhao *et al.*, 2008; Shin *et al.*, 2010; Murphy *et al.*, 2013; Walter *et al.*, 2018; Xie and Zhao, 2018), we confirmed that an explosion occurred at the NKTS at 3:30 a.m. on 3 September 2017. After about 8 min, the subsequent event was probably a collapse of the explosion cavity, and the remaining two aftershocks were likely tectonic earthquakes. Hereafter, we refer to these six successive North Korean nuclear tests as NKT1, NKT2, NKT3, NKT4, NKT5, and NKT6 for convenience.

HIGH-PRECISION RELATIVE LOCATION

The relative location method can provide accurate relative locations with respect to a master event by measuring the differential travel times of seismic waves (e.g., Schaff and Richards, 2004; Selby, 2010; Wen and Long, 2010; Murphy *et al.*, 2013; Zhao *et al.*, 2014, 2016; Zhao, Xie, He, *et al.*, 2017; Zhao, Xie, Wang, *et al.*, 2017; Pasyanos and Myers, 2018; Xie and Zhao, 2018). The CNDSN, GSN, FDSN, and F-net supplied an abundance of *Pn* waveforms, with good quality and no large azimuthal gaps, for all six North Korean nuclear tests, which is favorable for us to apply a relative location method to locate these explosions and their aftershocks with high precision. The source mechanisms for all explosions are highly similar. The *Pn* waveforms at a given station are very similar, with differential travel times between events, which is mostly due to their relative locations.

In this study, we extract *Pn* waveforms for six explosions from 255 stations. The cross-correlation calculations are then applied (Schaff and Richards, 2004; Zhao, Xie, Wang, *et al.*, 2017), resulting in 960 differential travel times. NKT1, whose location and origin time are obtained from satellite images and the USGS, respectively (Wen and Long, 2010; Zhao *et al.*, 2014), is assigned as the master event, and the *Pn*-wave velocity in the uppermost mantle beneath the NKTS is fixed to 7.99 km/s (e.g., Zhao *et al.*, 2016; Zhao, Xie, Wang, *et al.*, 2017). A relative location model is then created with 15 unknowns, including longitude, latitude, and origin time, for NKT2–NKT6. Considering the trade-off between depth and origin time, the burial depth is not included in the calculation. During the inversion, a larger search range, namely 20×20 km^2, is used for NKT6. For NKT2–NKT5, we use a smaller range of 2×2 km^2 centered at previously obtained epicenters. An annealing simulation method (Kirkpatrick *et al.*, 1983) is then performed to fit the observed *Pn* differential travel times, and the solution that minimizes the L2 norm for differences between the observed and synthetic *Pn* travel times contains the expected relative locations and origin times for the last five explosions. The relocated epicenters for NKT1–NKT6 are shown in Figure 3 and listed in Table 1. Although NKT1 was conducted at the southeast NKTS, NKT2–NKT6 moved westward toward a mountain ~2 km away. Derived from the error ellipse (Efron, 1983), the precision of the relative location of NKT6 is ~87 m. The relocation accuracy strongly relies on the location of the master event.

The above-mentioned seismic networks also recorded data from postexplosion events. Although the data quality is worse than that for the explosions, some *Pn* waveforms can be used to calculate cross-correlated differential travel times for relocation (Ⓔ Fig. S1 and Table S1, available in the electronic supplement to this article; Schaff and Richards, 2004; Zhao, Xie, Wang, *et al.*, 2017). However, because of their different mechanisms and epicentral locations, the correlation coefficients between the postexplosion events and explosions are significantly lower than those between the explosions themselves. After careful visual selection, the available differential travel times for the postexplosion events are far less than those for explosions. Therefore, when performing the relative location, we fix the previously obtained explosion locations to prevent potential measurement errors in the postexplosion events from propagating. The resultant locations of the postexplosion events show that the 3 September 2017 aftershock was very close to NKT6, with less than 200 m in between. The 23 September and 12 October 2017 aftershocks were clustered and located northeast of the NKTS more than 8 km from NKT6 (Fig. 3).

EVENT DISCRIMINATION

Discriminating underground nuclear tests from natural earthquakes relies on differences in the seismic waves that these two types of sources generate. The explosion source primarily generates *P* waves. In contrast, the earthquake source can be described as a dislocation, which generates an abundance of

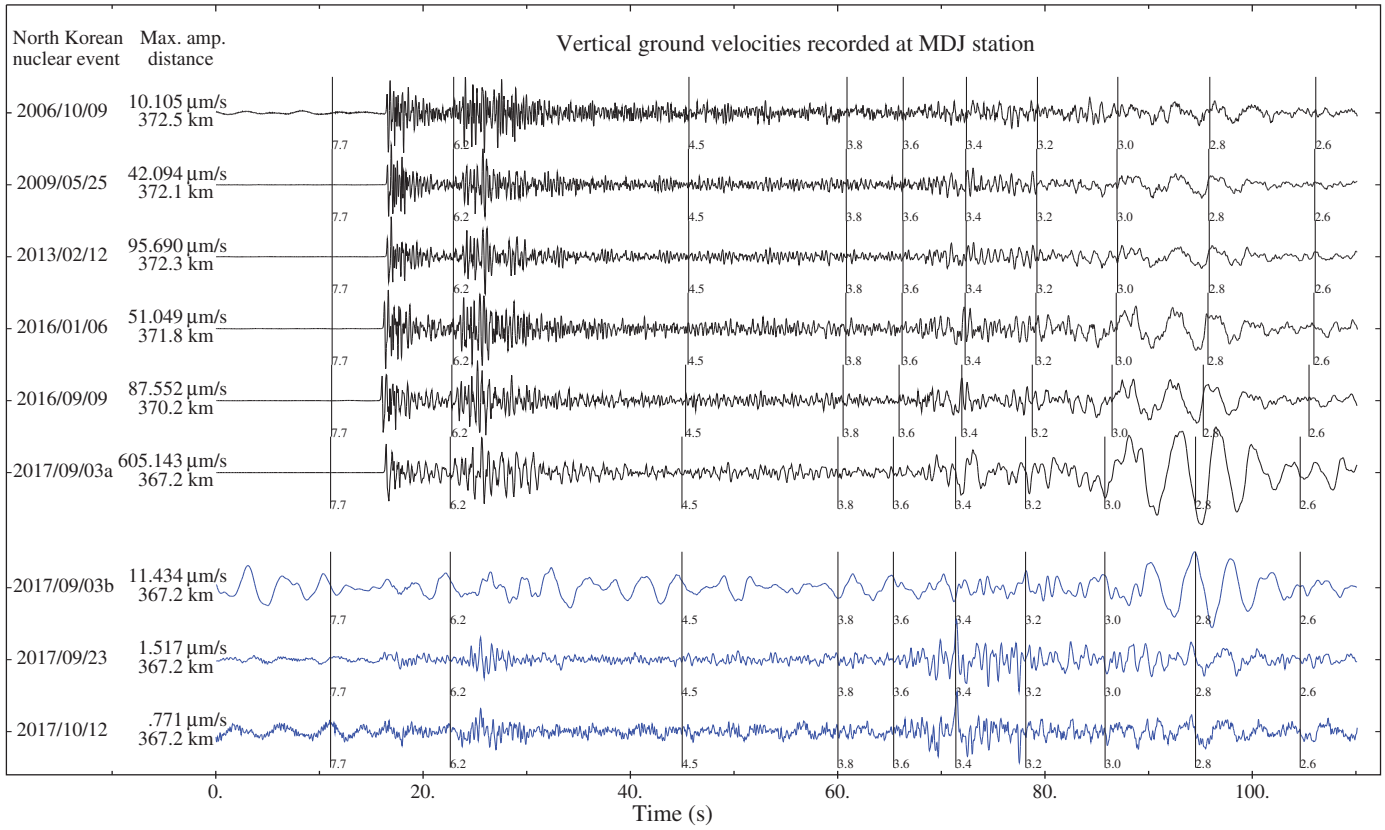

▲ **Figure 2.** Normalized vertical-component velocity seismograms recorded at MDJ station for the six known nuclear test explosions and for three aftershocks after the large test of 2017. The event dates, maximum amplitudes, and epicenter distances are listed on the left. The marks on the waveforms indicate the apparent group velocities. Whereas the seismograms for the explosions are characterized by impulsive *P*-wave onsets, relatively weak *Lg* phases, and 3- to 5-s short-period Rayleigh waves, the seismograms for the postexplosion events show different features, that is, lack of high-frequency content for the first aftershock, which may indicate that it was a collapse event, and amplitude differences between *P* and *S* waves for the other two aftershocks, which shows that they were unlikely to be explosions.

S waves but weak *P* waves. The *P*/*S* spectral ratios, through reducing effects from propagation and highlighting differences between source, can provide effective discrimination (e.g., Taylor *et al.*, 1989; Kim *et al.*, 1993; Walter *et al.*, 1995; Xie, 2002; Fisk, 2006; Walter *et al.*, 2007). For NKT1 on 9 October 2006, Richards and Kim (2007) determined that the event was an explosion based on the regional *P*/*S* spectral ratios. However, their results derived from single-station data were applicable only to the high-frequency spectra between 9.0 and 15.0 Hz. Taking advantage of digital broadband networks in northeast China, Zhao *et al.* (2008, 2014, 2016) and Zhao, Xie, Wang, *et al.* (2017) chose 11 high-quality stations with almost purely continental paths (Fig. 4a) and used seismograms to calculate spectral ratios *Pg*/*Lg*, *Pn*/*Lg*, and *Pn*/*Sn* (Hartse *et al.*, 1997). Then, based on magnitude and distance amplitude correction, spectral ratios from individual stations were corrected for trend versus distances at individual frequencies followed by calculating their averages (Walter *et al.*, 1995, 2007; Walter and Taylor, 2001; Zhao *et al.*, 2008). These network-averaged spectral ratios suppress data fluctuation and effectively expand the available frequency band for discrimination. With the modified method, all previous five North Korean nuclear explosions can be discriminated from natural earthquakes at frequencies higher than 2.0 Hz (Zhao *et al.*, 2008, 2014, 2016; Zhao, Xie, He, *et al.*, 2017; Zhao, Xie, Wang, *et al.*, 2017; Xie and Zhao, 2018).

For the suspected explosion on 3 September 2017 and three subsequent aftershocks, five previously confirmed North Korean nuclear explosions, and four nearby natural earthquakes, we calculate *P*/*S* spectral ratios *Pg*/*Lg*, *Pn*/*Lg*, and *Pn*/*Sn* from vertical-component waveforms at each of these 11 stations (Ⓔ Fig. S2). Spectral ratios *Pg*/*Lg* calculated at individual stations are shown in Figure 4b. Figure 4c shows the network-averaged *Pg*/*Lg* ratios for all five previous explosions and four natural earthquakes. The red and black dots and error bars are average values and standard deviations for all explosions and all earthquakes. They can be the templates for estimating properties of unknown events. Network-averaged spectral ratios *Pg*/*Lg*, *Pn*/*Lg*, and *Pn*/*Sn* for the 3 September 2017 main event and three subsequent aftershocks are illustrated in Figure 4d–f. For comparison, we also include average spectral ratios for all explosions and all earthquakes. The

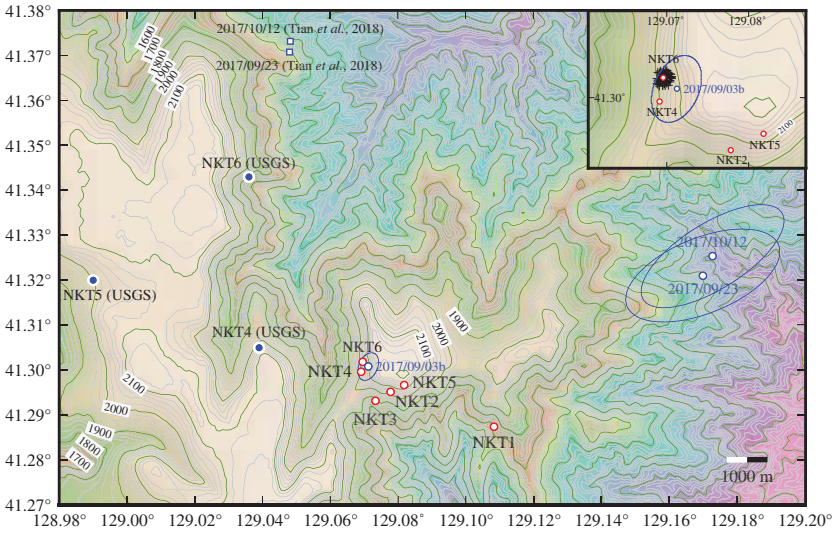

▲ **Figure 3.** Map showing the topography and relocated epicenters of the NKTS events. Open circles with blue error ellipses represent the results from this study, blue dots represent those given by the U.S. Geological Survey (USGS), and open squares represent the relocation results from Tian *et al.* (2018). The inset map zooms into the source region of NKT6, where crosses are epicenters obtained using partial information and used to estimate errors based on the bootstrap method (Efron, 1983).

spectral ratios of the 3 September 2017 main event are very close to the average values of NKT1–NKT5, indicating it is an explosion. The three postexplosion events exhibit rather complex patterns in their spectral ratios. Although they have generally lower values compared with typical explosions and are closer to the natural earthquakes, they show some special features and do not exactly fall into typical earthquake population. For the 3 September aftershock (blue lines in Fig. 4d–f), its spectral ratios at frequencies below 6 Hz are apparently higher than those from typical earthquakes. On the other hand, at frequencies higher than 6 Hz, its spectral ratios *Pg*/*Lg* and *Pn*/*Lg* become slightly lower than typical earthquakes (for *Pn*/*Sn* this happens above 10 Hz). Considering that this event is likely a collapse of the explosion cavity, the spectral ratio feature may be related to the collapse. However, these aftershocks have much shallower depth compared with natural earthquakes, so other factors may contribute to difference between these aftershocks and typical natural earthquakes.

DISCUSSIONS AND CONCLUSION

The regional waveforms generated by NKT6 exhibit striking similarities to those generated by NKT1–NKT5. *Pn* waveform cross-correlation calculation (Schaff and Richards, 2004; Zhao, Xie, Wang, *et al.*, 2017) generated 960 differential travel times, with which the epicenter of NKT6 was relocated and the epicenters of NKT2–NKT5 were updated (Zhao *et al.*, 2008, 2012, 2014, 2016; Zhao, Xie, He, *et al.*, 2017; Zhao, Xie, Wang, *et al.*, 2017; Xie and Zhao, 2018). We performed an annealing simulation (Kirkpatrick *et al.*, 1983) to minimize *Pn* differential travel times and searched for the optimal solution. The resultant epicenter for NKT6 is at 41.3018° N and 129.0696° E, locating on the west side of the mountain and ~3.6 km to the northwest of the master event NKT1. The updated locations for NKT2–NKT5 are consistent with those in the previous results (Zhao *et al.*, 2008, 2014, 2016; Zhao, Xie, He, *et al.*, 2017; Zhao, Xie, Wang, *et al.*, 2017). The relative location precision of NKT6 is ~87 m. However, its absolute uncertainty highly relies on the absolute location of the master event.

Compared with the epicenter from seismological methods, satellites can provide visual images of surface damage directly linked to the explosion. Based on the Mohr–Coulomb failure

Table 1
Best-Fit Locations and Origin Times for Events at the North Korean Nuclear Test Site

North Korea Nuclear Event	Date (yyyy/mm/dd)	Origin Time (hh:mm:ss.ssss)	Standard Deviation (s)	Latitude (°N)	Longitude (°E)	Location Uncertainty (m)
NKT1*	2006/10/09	01:35:28.0000*	0	41.2874†	129.1083†	Master event
NKT2	2009/05/25	00:54:43.1409	0.0170	41.2952	129.0778	52
NKT3	2013/02/12	02:57:51.2684	0.0070	41.2932	129.0733	52
NKT4	2016/01/06	01:30:00.9755	0.0059	41.2996	129.0691	70
NKT5	2016/09/09	00:30:01.3812	0.0044	41.2967	129.0818	32
NKT6	2017/09/03	03:30:01.6510	0.0051	41.3018	129.0696	87
PEV1	2017/09/03	03:38:32.7963	0.0914	41.3008	129.0712	360
PEV2	2017/09/23	08:29:15.9110	0.1320	41.3210	129.1700	2020
PEV3	2017/10/12	16:41:08.2134	0.1276	41.3253	129.1729	2020

NKT1, the first North Korean nuclear test; PEV1, the first postexplosion event.
*From U.S. Geological Survey.
†From satellite images (Wen and Long, 2010; Zhao *et al.*, 2014).

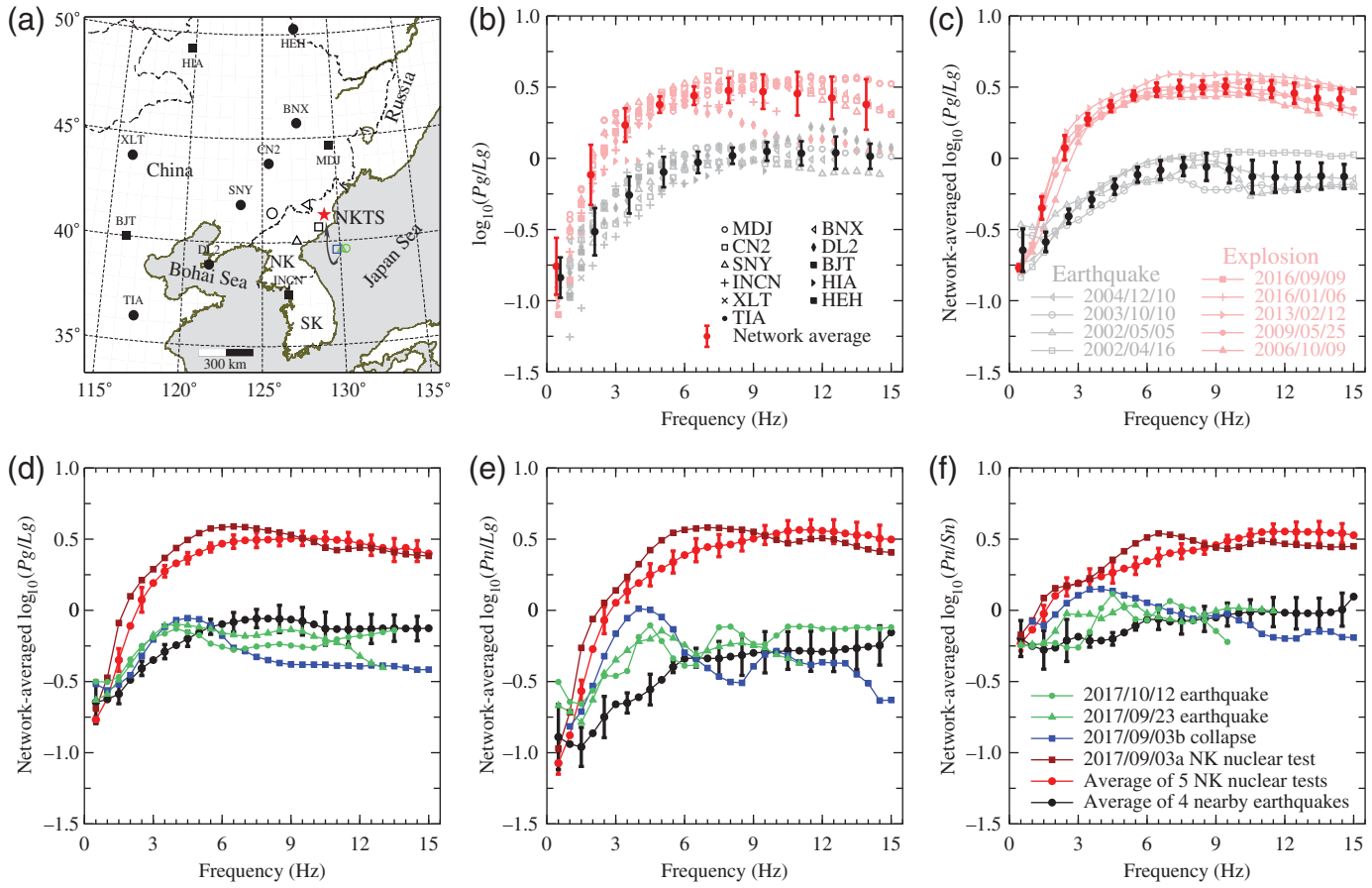

▲ **Figure 4.** (a) Map showing the locations of the NKTS (solid red star), station locations of the network for calculating the spectral ratios (solid black squares and circles), epicenters of the four natural earthquakes (open circles, triangles, and squares), and three unidentified aftershocks (blue square, green triangle, and circle). (b) *Pg*/*Lg* spectral ratios from individual stations and network averages. (c) Light colored symbols and curves are network-averaged spectral ratios for five known explosions and four natural earthquakes. Red and black dots and curves are averages from all known explosions and all nature earthquakes. They represent typical spectral ratios for explosions and earthquakes. The error bars are their standard deviations. (d–f) Network-averaged spectral ratios for NKT6 and three aftershocks. For comparison, typical spectral ratios for explosions and earthquakes, along with their error bars, are also presented in these figures.

criterion, surface materials can fail when the shear stress exceeds its shear strength, and failure is more likely to happen at the critical point where existing shear stress approaches to the shear strength such as on the peak of a mountain or the edge of a steep slope. This makes using satellite image to locate a large explosion such as NKT6 tricky. A large explosion can create stress variations extended far away from the epicenter. For example, NKT6 caused substantial surface disturbance over an area of ~9 km^2, where large displacements occurred on the west and south flanks, and debris flows were localized in pre-existing channels (Pabian and Coblentz, 2018; Wang *et al.*, 2018). The center of the explosion cannot be easily determined from these spatially distributed phenomena. In contrast, a small explosion such as NKT1 tends to produce more localized surface damage above the epicenter. Therefore, despite a considerable signal-to-noise ratio, we prefer to use NKT1 as the master event for the relative location.

The *P*/*S* spectral ratios, including *Pg*/*Lg*, *Pn*/*Lg*, and *Pn*/*Sn*, are calculated using an 11-station network. All three types of network-averaged spectral ratios show that the mainshock on 9 September 2017 unambiguously belongs to the explosion population, confirming it was the sixth North Korean nuclear test. The results also suggest that network-averaged *P*/*S* spectral ratios, when used as discriminant in the China–North Korea border area, can reduce data fluctuation and expand the available frequency band to 2.0 Hz at the low-frequency end (Kim *et al.*, 1993; Richards and Kim, 2007; Zhao *et al.*, 2008, 2012, 2014, 2016; Zhao, Xie, He, *et al.*, 2017; Zhao, Xie, Wang, *et al.*, 2017; Xie and Zhao, 2018). Even corrected by the epicenter distances, there is noticeable scattering in the current *P*/*S* ratio measurements. This is largely due to the range of event magnitudes used and complicated local geology. To further improve the result, observed spectra for different phases should be corrected for magnitude and 2D regional attenuation models before calculating the spectral ratios (e.g., Fisk, 2006; Murphy *et al.*, 2009; Fisk and Pasyanos, 2016).

NKT6 was followed by three aftershocks, which occurred on 3 September, 8.5 min after the main event, and on

23 September and 12 October 2017 with decreasing magnitudes of $M_L = 4.1$, 3.5, and 2.9, respectively. Their waveforms exhibit significant differences from explosion seismograms (Fig. 2) because their *P* waves are relatively weak, but the *Lg* waves are strong. The *P*/*S* spectral ratios demonstrated that these aftershocks can be excluded from the explosion population but do not exactly fall onto spectral ratio population for natural earthquakes (Fig. 4d,e). Our relocation results show that the first aftershock was within 200 m from NKT6, indicating it is possibly due to a collapse of the explosion cavity. Based on intermediate-period regional wave modeling, both Liu *et al.* (2018) and Tian *et al.* (2018) obtained similar focal mechanisms for the first aftershock. Compared with the natural earthquake, its spectral ratios have prominent features, which may be related to its collapse mechanism. Using satellite radar imagery, Wang *et al.* (2018) revealed substantial surface subsidence of about 0.5 m at the NKTS, which may be related to cavity collapse. For the two latter aftershocks, Tian *et al.* (2018) and Yao *et al.* (2018) suggested that they were about 8 km north of NKT6. Kim *et al.* (2018) and Schaff *et al.* (2018) reported that there were a cluster of small earthquakes, northeast–southwest aligned and located north-northeast to NKT6, including the two above-mentioned later aftershocks. However, our relocation revealed that these two aftershocks were located over 8 km northeast of NKT6 (see comparisons in Fig. 3). The source mechanisms of three aftershocks are apparently different from those explosions and possibly different from each other. In addition, their seismograms show low signal-to-noise ratios because of the low magnitudes. The resultant low waveform consistency between explosions and aftershocks brought large errors in calculating differential travel times, causing relocation uncertainties between aftershocks and explosions. Nevertheless, all authors agreed that the first aftershock was under the same mountain as NKT6, and the remaining two aftershocks may have occurred several kilometers away from NKT6. Therefore, these two later aftershocks were unlikely directly related to NKT6. The spectral ratios from these two aftershocks are somewhat in between that from the first aftershock and typical natural earthquake. Because of limited information, the mechanisms of these two aftershocks are not clear. They may result from mechanisms such as a landslide or collapse or maybe just because they have very shallow sources compared with the depth of typical tectonic earthquakes. Future investigations are required for these aftershocks.

DATA AND RESOURCES

The waveforms recorded at the China National Digital Seismic Network (CNDSN), Global Seismic Network (GSN), International Federation of Digital Seismograph Networks (FDSN), and Full Range Seismograph Network (F-net) stations used in this study were collected from the China Earthquake Network Center (CENC), the Data Management Centre of China National Seismic Network at the Institute of Geophysics, China Earthquake Administration (SEIDMC; Zheng *et al.*, 2010) at http://www.seisdmc.ac.cn (last accessed July 2018), the Incorporated Research Institutions for Seismology Data Management Center (IRIS-DMC) at www.iris.edu (last accessed July 2018), and the National Research Institute for Earth Science and Disaster Prevention (NIED) at http://www.fnet.bosai.go.jp (last accessed July 2018).

ACKNOWLEDGMENTS

Editor-in-Chief Z. Peng, Guest Editor W. R. Walter, and reviewers P. G. Richards and M. E. Pasyanos are appreciated for their comments that greatly improved this article. This research was supported by the National Key Research and Development Program of China (Grant 2017YFC0601206) and the National Natural Science Foundation of China (Grants 41674060 and 41630210). Certain figures were generated using the Generic Mapping Tools (GMT; Wessel and Smith, 1998).

REFERENCES

Efron, B. (1983). Estimating the error rate of a prediction rule: Improvement on cross-validation, *J. Am. Stat. Assoc.* **78,** 316–331, doi: 10.2307/2288636.

Fisk, M. D. (2006). Source spectral modeling of regional *P/S* discriminants at nuclear test sites in China and the former Soviet Union, *Bull. Seismol. Soc. Am.* **96,** 2348–2367, doi: 10.1785/0120060023.

Fisk, M. D., and M. E. Pasyanos (2016). Significantly improving regional seismic amplitude tomography at higher frequencies by determining *S*-wave bandwidth, *Bull. Seismol. Soc. Am.* **106,** 928–942, doi: 10.1785/0120150247.

Hartse, H. E., S. R. Taylor, W. S. Phillips, and G. E. Randall (1997). A preliminary study of regional seismic discrimination in central Asia with emphasis on western China, *Bull. Seismol. Soc. Am.* **87,** 551–568.

Kim, W. Y., P. G. Richards, D. P. Schaff, E. Jo, and Y. Ryoo (2018). Identification of seismic events on and near the North Korean test site following the underground nuclear test explosion of 3 September 2017, *Seismol. Res. Lett.* doi: 10.1785/0220180133 (this volume).

Kim, W. Y., D. W. Simpson, and P. G. Richards (1993). Discrimination of earthquakes and explosions in the eastern United States using regional high-frequency data, *Geophys. Res. Lett.* **20,** 1507–1510, doi: 10.1029/93gl01267.

Kirkpatrick, S., C. D. Gelatt Jr., and M. P. Vecchi (1983). Optimization by simulated annealing, *Science* **220,** 671–680, doi: 10.1126/science.220.4598.671.

Liu, J., L. Li, J. Zahradnik, E. Sokos, C. Liu, and X. Tian (2018). North Korea's 2017 test and its nontectonic aftershock, *Geophys. Res. Lett.* **45,** 3017–3025, doi: 10.1002/2018GL077095.

Murphy, J. R., B. W. Barker, D. D. Sultanov, and O. P. Kuznetsov (2009). *S*-wave generation by underground explosions: Implications from observed frequency-dependent source scaling, *Bull. Seismol. Soc. Am.* **99,** 809–829, doi: 10.1785/0120080126.

Murphy, J. R., J. L. Stevens, B. C. Kohl, and T. J. Bennett (2013). Advanced seismic analyses of the source characteristics of the 2006 and 2009 North Korean nuclear tests, *Bull. Seismol. Soc. Am.* **103,** 1640–1661, doi: 10.1785/0120120194.

Pabian, F., and D. Coblentz (2018). Observed surface disturbances associated with the DPRK's 3 September 2017 underground nuclear test, *Seismol. Res. Lett.* doi: 10.1785/0220180120 (this volume).

Pasyanos, M. E., and S. C. Myers (2018). The coupled location/depth/yield problem for North Korea's declared nuclear tests, *Seismol. Res. Lett.* doi: 10.1785/0220180109 (this volume).

Richards, P. G., and W. Y. Kim (2007). Seismic signature, *Nature Phys.* **3,** 4–6, doi: 10.1038/nphys495.

Schaff, D. P., and P. G. Richards (2004). Repeating seismic events in China, *Science* **303,** 1176–1178, doi: 10.1126/science.1093422.

Schaff, D. P., W. Y. Kim, P. G. Richards, E. Jo, and Y. Ryoo (2018). Using waveform cross correlation for detection, location, and identification of aftershocks of the 2017 nuclear explosion at the North Korea test site, *Seismol. Res. Lett.* doi: 10.1785/0220180132 (this volume).

Schlittenhardt, J., M. Canty, and I. Grunberg (2010). Satellite earth observations support CTBT monitoring: A case study of the nuclear test in North Korea of Oct. 9, 2006 and comparison with seismic results, *Pure Appl. Geophys.* **167,** 601–618, doi: 10.1007/s00024-009-0036-x.

Selby, N. D. (2010). Relative locations of the October 2006 and May 2009 DPRK announced nuclear tests using international monitoring system seismometer arrays, *Bull. Seismol. Soc. Am.* **100,** 1779–1784, doi: 10.1785/0120100006.

Shin, J. S., D. H. Sheen, and G. Kim (2010). Regional observations of the second North Korean nuclear test on 2009 May 25, *Geophys. J. Int.* **180,** 243–250, doi: 10.1111/j.1365-246X.2009.04422.x.

Taylor, S. R., M. D. Denny, E. S. Vergino, and R. E. Glaser (1989). Regional discrimination between NTS explosions and western United States earthquakes, *Bull. Seismol. Soc. Am.* 79**,** 1142–1176.

Tian, D. D., J. Y. Yao, and L. X. Wen (2018). Collapse and earthquake swarm after North Korea's 3 September 2017 nuclear test, *Geophys. Res. Lett.* **45,** 3976–3983, doi: 10.1029/2018GL077649.

Walter, W. R., and S. R. Taylor (2001). A revised magnitude and distance amplitude correction (MDAC2) procedure for regional seismic discriminants: Theory and testing at NTS, *Technical Report*, doi: 10.2172/15013384.

Walter, W. R., D. A. Dodge, G. Ichinose, S. C. Myers, M. E. Pasyanos, and S. R. Ford (2018). Body-wave method of distinguishing between explosions, collapse and earthquakes—Application to recent events in North Korea, *Seismol. Res. Lett.* doi: 10.1785/0220180128 (this volume).

Walter, W. R., E. Matzel, M. E. Pasyanos, D. B. Harris, R. Gok, and S. R. Ford (2007). Empirical observations of earthquake-explosion discrimination using P/S ratios and implications for the sources of explosion *S*-waves, *29th Monitoring Research Review: Ground-Based Nuclear Explosion Monitoring Technologies*, Denver, Colorado, 25–27 September 2007, 684–693.

Walter, W. R., K. M. Mayeda, and H. J. Patton (1995). Phase and spectral ratio discrimination between NTS earthquakes and explosions. Part I: Empirical observations, *Bull. Seismol. Soc. Am.* **85,** 1050–1067.

Wang, T., Q. Shi, M. Nikkhoo, S. Wei, S. Barbot, D. Dreger, R. Burgmann, M. Motagh, and Q. F. Chen (2018). The rise, collapse, and compaction of Mt. Mantap from the 3 September 2017 North Korean nuclear test, *Science* **361,** 166–170, doi: 10.1126/science.aar7230.

Wen, L. X., and H. Long (2010). High-precision location of North Korea's 2009 nuclear test, *Seismol. Res. Lett.* **81,** 26–29, doi: 10.1785/gssrl.81.1.26.

Wessel, P., and W. H. F. Smith (1998). New, improved version of generic mapping tools released, *Eos Trans. AGU* **79,** 579, doi: 10.1029/98eo00426.

Xie, J. K. (2002). Source scaling of *Pn* and *Lg* spectra and their ratios from explosions in central Asia: Implications for the identification of small seismic events at regional distances, *J. Geophys. Res.* **107,** doi: 10.1029/2001jb000509.

Xie, X. B., and L. F. Zhao (2018). The seismic characterization of North Korea underground nuclear tests, *Chin. J. Geophys.* **61,** 889–904, doi: 10.6038/cjg2018L0677 (in Chinese).

Yao, J. Y., D. D. Tian, Z. Lu, L. Sun, and L. X. Wen (2018). Triggered seismicity after North Korea's 3 September 2017 nuclear test, *Seismol. Res. Lett.* doi: 10.1785/0220180135 (this volume).

Zhang, M., and L. X. Wen (2013). High-precision location and yield of North Korea's 2013 nuclear test, *Geophys. Res. Lett.* **40,** 2941–2946, doi: 10.1002/grl.50607.

Zhao, L. F., X. B. Xie, X. He, X. Zhao, and Z. X. Yao (2017). Seismological discrimination and yield estimation of the 3 September 2017 Democratic People's Republic of Korea (DPRK) underground nuclear test, *Chin. Sci. Bull.* **62,** 4163–4168, doi: 10.1360/N972017-00979 (in Chinese).

Zhao, L. F., X. B. Xie, W. M. Wang, N. Fan, X. Zhao, and Z. X. Yao (2017). The 9 September 2016 North Korean underground nuclear test, *Bull. Seismol. Soc. Am.* **107,** 3044–3051, doi: 10.1785/0120160355.

Zhao, L. F., X. B. Xie, W. M. Wang, J. L. Hao, and Z. X. Yao (2016). Seismological investigation of the 2016 January 6 North Korean underground nuclear test, *Geophys. J. Int.* **206,** 1487–1491, doi: 10.1093/gji/ggw239.

Zhao, L. F., X. B. Xie, W. M. Wang, and Z. X. Yao (2008). Regional seismic characteristics of the 9 October 2006 North Korean nuclear test, *Bull. Seismol. Soc. Am.* **98,** 2571–2589, doi: 10.1785/0120080128.

Zhao, L. F., X. B. Xie, W. M. Wang, and Z. X. Yao (2012). Yield estimation of the 25 May 2009 North Korean nuclear explosion, *Bull. Seismol. Soc. Am.* **102,** 467–478, doi: 10.1785/0120110163.

Zhao, L. F., X. B. Xie, W. M. Wang, and Z. X. Yao (2014). The 12 February 2013 North Korean underground nuclear test, *Seismol. Res. Lett.* **85,** 130–134, doi: 10.1785/0220130103.

Zheng, X. F., Z. X. Yao, J. H. Liang, and J. Zheng (2010). The role played and opportunities provided by IGP DMC of China National Seismic Network in Wenchuan earthquake disaster relief and researches, *Bull. Seismol. Soc. Am.* **100,** 2866–2872, doi: 10.1785/0120090257.

Xi He[1]
Lian-Feng Zhao
Zhen-Xing Yao
Key Laboratory of Earth and Planetary Physics
Institute of Geology and Geophysics, Chinese Academy of Sciences
19 Beitucheng West Road, Chaoyang District
Beijing 100029, China
zhaolf@mail.iggcas.ac.cn
hexi@mail.iggcas.ac.cn
yaozx@mail.iggcas.ac.cn

Xiao-Bi Xie
Institute of Geophysics and Planetary Physics
University of California at Santa Cruz
1156 High Street
Santa Cruz, California 95064 U.S.A.
xxie@ucsc.edu
yaozx@mail.iggcas.ac.cn

Published Online 26 September 2018

[1] Also at College of Earth and Planetary Sciences, University of Chinese Academy of Sciences, Beijing 100049, China.